Quantum phase transitions in driven Fock-state lattices with synthetic gauge fields

Jiale Yuan,[1,*] Jinfeng Deng,[1] Xiao Wei,[1] and Da-Wei Wang[1,2,3,†]

[1]*Zhejiang Key Laboratory of Micro-Nano Quantum Chips and Quantum Control, School of Physics, and State Key Laboratory for Extreme Photonics and Instrumentation, Zhejiang University, Hangzhou 310027, China*

[2]*College of Optical Science and Engineering, Zhejiang University, Hangzhou 310027, China*

[3]*Hefei National Laboratory, Hefei 230088, Anhui Province, China*

(Received 21 July 2025; accepted 1 November 2025; published 20 November 2025)

Quantum phase transitions (QPTs) typically emerge in the thermodynamic limit, yet a single-atom QPT can arise when it is coupled to a coherently driven cavity, which provides a simple and unique platform to engineer quantum states with quantum criticality. In this driven Jaynes-Cummings (JC) model, the cavity field becomes squeezed near the critical point. However, vanishing energy gaps at the critical points lead to nonadiabaticity, hindering the practical realization of squeezing. In this work, we introduce a spin-dependent cavity drive, which induces a synthetic gauge field in the Fock-state lattice and enriches the phase diagram of the driven JC model. Remarkably, the energy spectrum can remain discrete for all driving strengths, allowing an adiabatic preparation of squeezed states with robust energy gaps. Moreover, we identify a topological phase transition characterized by projected winding numbers in the presence of broken chiral symmetry. Our results unveil topology and QPTs in a quantized light-matter system and offer a robust strategy for realizing squeezed states.

DOI: 10.1103/4fq1-nb4r

I. INTRODUCTION

Quantum phase transitions (QPTs) are marked by abrupt changes in the energy spectrum of a many-body Hamiltonian as system parameters are continuously tuned. Traditionally, QPTs arise in the thermodynamic limit, where the number of particles diverges, as exemplified by quantum ferromagnetic transitions [1] and superconductor-insulator transitions [2]. Remarkably, superradiant phase transitions [3–6] can occur even in the single-atom limit, as demonstrated in the Jaynes-Cummings (JC) model both with [7] and without [8–11] the rotating-wave approximation. In the undriven JC model, realizing such a transition in the single-atom limit requires the atomic transition frequency to greatly exceed the cavity resonance frequency. Interestingly, this constraint is lifted when the cavity is coherently driven [12,13]. The driven JC model features two distinct quantum phases, one with discrete and the other with continuous energy spectra, depending on the ratio between the driving strength and the atom-cavity coupling strength. Above a finite critical ratio, bimodal cavity field emerges in the dissipative regime [14–16]. Below this threshold, analytic eigenstates can be obtained, and the cavity field exhibits strong squeezing near the critical point [13,17], offering a route for the adiabatic preparation of highly squeezed states. These states offer a valuable quantum resource with applications in high-precision measurements [18–23], entangled-based quantum key distribution [24,25], and fundamental tests of quantum mechanics [26,27]. However, the energy gap closing at the critical point requires an infinitely slow evolution to remain adiabatic [28–31], which is infeasible in practice due to the finite coherence time of realistic quantum systems.

Fock-state lattices (FSLs) [32–35] have recently emerged as a powerful platform for exploring a wide range of QPTs [36–39]. In particular, the introduction of synthetic gauge fields in FSLs [38–40] has enabled the realization of quantum phases with direct analogs in condensed matter systems, significantly enriching the phase diagram of the JC model [33,41–44]. In this article, we incorporate an atomic state-dependent cavity driving field [39] into the JC model to investigate its quantum and topological phase transitions, along with their implications for adiabatic cavity field squeezing. The atomic state-dependent drive introduces a synthetic gauge field in the FSL framework, thus extending the parameter space of the driven JC model [12,13] through the addition of a tunable synthetic magnetic flux. At a flux of π per unit cell, the system exhibits fully discrete energy spectra for any driving strength, ensuring that the adiabatic condition for cavity field squeezing can always be fulfilled. Moreover, we discover a topological phase transition characterized by a projected winding number [45] that emerges when the chiral (sublattice) symmetry is broken. This reveals a highly tunable platform for investigating generalized topological phases and bulk-edge correspondence in quantized light-matter systems. Altogether, our work sheds light on both symmetry-breaking and topological phase transitions in cavity quantum electrodynamic systems and offers a robust and scalable

*Contact author: jialeyuan@zju.edu.cn

†Contact author: dwwang@zju.edu.cn

Published by the American Physical Society under the terms of the Creative Commons Attribution 4.0 International license. Further distribution of this work must maintain attribution to the author(s) and the published article's title, journal citation, and DOI.

strategy for generating squeezed states through adiabatic evolution.

II. MODEL

We consider a JC model incorporating resonant drives on both the atom (represented as a pseudospin) and cavity, along with an additional spin-dependent cavity drive. In the interaction picture, the system is governed by the Hamiltonian

$$H_0 = g(\sigma^+ a + \sigma^- a^\dagger) + (\eta\sigma^+ + \eta^*\sigma^-) + (\varepsilon a^\dagger + \varepsilon^* a) + \sigma_z(\kappa a^\dagger + \kappa^* a), \quad (1)$$

where g is the vacuum Rabi frequency between the spin and cavity, η is the coherent driving field strength of the spin, ε is the coherent driving strength of the cavity, and κ is the coupling strength between the cavity field and σ_z. The κ term can be introduced by the simultaneous Floquet modulation of the vacuum Rabi frequency and spin driving field strength with a phase difference, $\tilde{g}(t) = g + \Delta_1\cos(\nu t + \phi_1)$ and $\tilde{\eta}(t) = \eta + \Delta_2\cos(\nu t + \phi_2)$, resulting in $\kappa = i\Delta_1\Delta_2\sin(\phi_2 - \phi_1)/(2\nu)$ [38,46–48] (see the Supplemental Material [49]). The last two terms in Eq. (1) contribute to an effective gauge field [see Fig. 1(c)]. This gauge field can be generated alternatively from the quantum Rabi model in a transformed frame [39].

To diagonalize this model, we make a transformation to absorb the spin driving term $H_1 = D^\dagger(\alpha_s)H_0D(\alpha_s)$, where $D(\alpha) = \exp(\alpha a^\dagger - \alpha^* a)$ and $\alpha_s = -\eta/g$. We obtain

$$H_1 = \frac{\Delta}{2}\sigma_z + g(\sigma^+ a + \sigma^- a^\dagger) + (\varepsilon a^\dagger + \varepsilon^* a) + \sigma_z(\kappa a^\dagger + \kappa^* a) + (\varepsilon\alpha_s^* + \varepsilon^*\alpha_s), \quad (2)$$

where $\Delta = 2(\kappa\alpha_s^* + \kappa^*\alpha_s)$ is a detuning in the displaced frame. The last term in Eq. (2) is a constant energy shift and we neglect it in the following discussion. The displaced Hamiltonian (2) can then be diagonalized analytically [13] (see the Supplemental Material [49] for details). As a result, we find that the energy spectra can be categorized into two phases characterized by a discrete and a continuous energy spectrum, respectively, with the phase transition condition,

$$G = g^2\sqrt{\frac{1}{4} - \Re^2\tan^2\Phi} - \Re = 0, \quad (3)$$

where $\Phi = \arg[\varepsilon + \kappa] + \arg[\varepsilon^* - \kappa^*]$ is the synthetic magnetic flux, which accounts for the accumulated phase in a unit cell in the FSL, as shown in Fig. 1(c), and $\Re = (|\varepsilon|^2 - |\kappa|^2)/g^2$. When $G^2 > 0$, we obtain the quantized energies

$$E_n^\pm = \frac{1}{g^4 + 4g^2|\kappa|^2}[-g^2\Delta(\varepsilon\kappa^* + \kappa\varepsilon^*) \pm \sqrt{g^4\Delta^2G^2 + 8g^2(g^2 + 4|\kappa|^2)G^3n}] \quad (4)$$

for $n \geqslant 1$ and $E_0 = -\Delta(\varepsilon\kappa^* + \kappa\varepsilon^* + G)/(g^2 + 4|\kappa|^2)$. When $G^2 < 0$, the spectra become continuous.

We show the phase diagram in Fig. 1(a), where the blue and red areas represent the discrete and continuous phases, respectively. The white areas are forbidden, since for $\pi/2 < \Phi < 3\pi/2$ we have $|\kappa| > |\varepsilon|$ and thus $\Re < 0$. In the rest region, we have $\Re > 0$. The resulting phase diagram extends the well-known critical point of the driven JC model at $\Phi = 0$ and $\Re = 1/4$ [12–14,17]. In contrast to the conventional cavity drive, the spin-dependent driving term can avoid the energy gap closures in the JC model. This is clearly demonstrated in the phase diagram at $\Phi = \pi$, where the system remains entirely within the discrete-spectrum phase (highlighted by the yellow dashed line). For other values of flux, quantum phase transitions occur at finite driving strengths. As a representative case, we plot the energy spectra in Fig. 1(b) using parameters $\varepsilon = g\cos(\Phi/2)$ and $\kappa = ig\sin(\Phi/2)$, corresponding to the black solid line in Fig. 1(a). Within the interval bounded by the two critical fluxes $\Phi = 2\pi/3$ and $\Phi = 4\pi/3$, the system supports discrete eigenenergies with level splittings scaling as $\sqrt{n}$ in the resonant case ($\Delta = 0$).

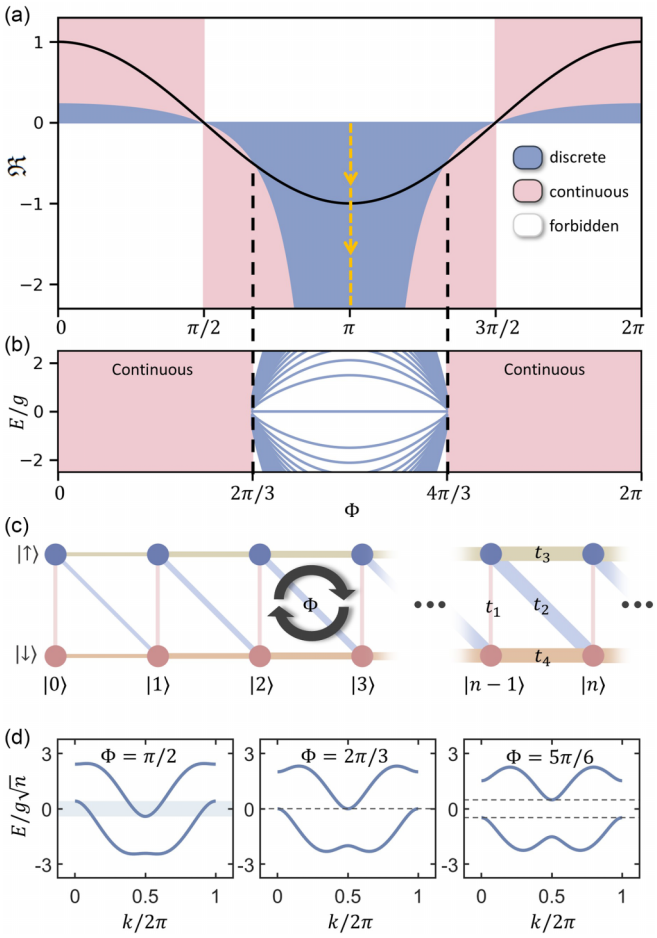


FIG. 1. The quantum phase transition in a driven Fock-state lattice with gauge field. (a) Phase diagram as a function of the flux Φ and $\Re$. The blue (red) areas represent the discrete (continuous) phase. The white areas are forbidden for system parameters. The dashed yellow line shows the adiabatic path for cavity field squeezing. (b) Energy spectra with parameters on the black solid line in panel (a), constrained by $\varepsilon = g\cos(\Phi/2)$ and $\kappa = ig\sin(\Phi/2)$. (c) The FSL of the driven JC model with a synthetic gauge field. The blue and red sites stand for $\uparrow$ and $\downarrow$ sublattices, respectively. Each unit cell hosts a magnetic flux Φ. The widths of the lines are proportional to the coupling strengths. (d) The quasimomentum-space spectrum with $\Phi = \pi/2, 2\pi/3$ (critical point), and $5\pi/6$.

The QPT can be intuitively understood from the FSL perspective. The Hamiltonian in Eq. (1) maps onto a

one-dimensional semi-infinite ladder [Fig. 1(c)], constructed from the Fock states of the combined spin-cavity system. The two sublattices, corresponding to the spin states ↑ and ↓, are indicated by blue and red sites, respectively. The lattice coordinate is defined by the photon number in the cavity, with the position operator given by $x = a^\dagger a$. In this lattice picture, intracell couplings t_1 arise from the spin drive, while nearest-neighbor intercell couplings t_3 and t_4 are generated by the cavity drive and the synthetic gauge field. The next-nearest-neighbor hopping terms t_2 are induced by the JC coupling.

The photon-number dependence of t_j's breaks the translational symmetry. To analyze our model from a lattice view, we adapt the momentum-space Hamiltonian of a periodic ladder sharing the same lattice structure of our FSL, with its constant couplings replaced by the local coupling strengths of the FSL [33,50–52]. This leads to the quasimomentum-space Hamiltonian (see the Supplemental Material [49] for its derivation),

$$H_n(k) = \mathrm{Re}[(t_3 + t_4)e^{-ik}] + \mathbf{d}_n(k)\cdot\boldsymbol{\sigma}, \tag{5}$$

where the vector $\mathbf{d}_n(k) = (\mathrm{Re}[t_2 e^{ik} + t_1],\ -\mathrm{Im}[t_2 e^{ik} + t_1],\ \mathrm{Re}[(t_3 - t_4)e^{-ik}])$ is an effective field in the pseudospin space, $\boldsymbol{\sigma}$ denotes the Pauli matrix vector, and k is a quasimomentum parameter, which can be considered as the phase of the semiclassical field resulting from the virtual lattice extension. The hopping amplitudes are given by $t_1 = \eta$, $t_2 = g\sqrt{n}$, $t_3 = (\varepsilon + \kappa)\sqrt{n}$, and $t_4 = (\varepsilon - \kappa)\sqrt{n}$, as shown in Fig. 1(c). In the limit $n \to \infty$, the Hamiltonian has two energy bands,

$$\frac{E^{\pm}(k)}{\sqrt{n}} = 2\mathrm{Re}[\varepsilon e^{-ik}] \pm \sqrt{g^2 + 4\mathrm{Re}[\kappa e^{-ik}]^2}. \tag{6}$$

Figure 1(d) shows the resulting band structures for three different flux values, $\Phi = \pi/2$, $2\pi/3$, and $5\pi/6$, with $\varepsilon = g\cos(\Phi/2)$ and $\kappa = ig\sin(\Phi/2)$. At $\Phi = \pi/2$, the two bands overlap in energy, corresponding to the continuous-spectrum phase. In contrast, a finite bandgap appears at $\Phi = 5\pi/6$, characteristic of the discrete-spectrum phase. At the critical point $\Phi = 2\pi/3$, the bandgap closes, signaling a QPT. Thus, in the limit $n \to \infty$, the transition between discrete and continuous energy spectra manifests as a transition between insulating and metallic band structures (see the Supplemental Material [49] for details).

III. CAVITY FIELD SQUEEZING

The cavity field can be squeezed during the adiabatic process approaching the critical point. The zeroth eigenstate of Hamiltonian (2) in the discrete phase is $|\psi_0\rangle = D(\alpha_0)S(\beta)|0\rangle \otimes |\sigma_0\rangle$, where $S(\beta) = \exp[(\beta^* a^2 - \beta a^{\dagger 2})/2]$, and the displacement and the squeezing parameters are

$$\alpha_0 = \frac{\Delta(2\varepsilon|\kappa|^2 + g^2\varepsilon - 2\varepsilon^*\kappa^2)}{2G(g^2 + 4|\kappa|^2)} - \frac{\Delta\kappa}{g^2 + 4|\kappa|^2}, \tag{7a}$$

$$\beta = \sinh^{-1}\left[-\sqrt{-\frac{1}{2} + \frac{g^2}{2G}\left(\frac{1}{2} - \Re\right)}\right] e^{i\cdot\arg[\varepsilon^2 - \kappa^2]}. \tag{7b}$$

The squeezing degree, a measure of the noise reduction of a quadrature below the standard quantum limit, is proportional to the squeezing parameter $\mathrm{SD} = 8.686|\beta|$. The spin state is

$$|\sigma_0\rangle = c_n\left(-G - \varepsilon\kappa^* + \kappa\varepsilon^* - \frac{g^2}{2}\right)|\downarrow\rangle + c_n g(\varepsilon - \kappa)|\uparrow\rangle, \tag{8}$$

where c_n is a normalization factor (see other eigenstates in the Supplemental Material [49]). For this eigenstate, the cavity field is squeezed, displaced, and disentangled from the spin.

As the system approaches the critical point $G \to 0$, the squeezing parameter diverges ($|\beta| \to \infty$), indicating the potential for generating highly squeezed states by initializing the system in the vacuum and adiabatically ramping up the driving fields toward the transition point. However, the vanishing energy gap at the critical point challenges such adiabatic processes. The synthetic gauge field offers an adiabatic path that can achieve strong squeezing while maintaining adiabaticity through increasing $|\kappa|/g$, with the system driven along the yellow dashed line at $\Phi = \pi$ in Fig. 1(a). To achieve large $|\kappa|/g$, we can tune the system parameters as $\kappa = ig_0[1 - \exp(-0.01t)]$ and $g = g_0\exp(-0.007t)$ with $g_0 = 2\pi \times 10\,\mathrm{MHz}$ [see Fig. 2(a)], which are within experimentally achievable ranges. Figure 2(b) displays the squeezing degree as a function of time in this scheme (solid blue curve), which achieves a maximum squeezing degree of approximately 18 dB. For comparison, in the $\Phi = 0$ scenario, only a squeezing degree of 6.8 dB is attained, where the system parameters are tuned as $g = g_0$ and $\varepsilon = 0.5g_0[1 - \exp(-0.01t)]$. In this case, the adiabatic condition breaks down after around 400 ns, as evidenced by the deviation of the simulated curve (solid red line) from the ideal values (dashed red line) that are evaluated by the system instantaneous eigenstates.

IV. CRITICAL SPIN POLARIZATION AND FIELD BIMODALITY

At the QPT point, the spin becomes disentangled from the cavity field (see the Supplemental Material [49]). The resulting critical spin polarization is remarkably robust against both nonadiabatic effects and dissipation, making it a valuable resource for quantum metrology [17]. In general, the critical spin wave function can be obtained by taking the limit $G \to 0$ in Eq. (8). We focus on a specific case where the driving parameters are chosen as $\varepsilon = \zeta g\cos(\Phi/2)$ and $\kappa = i\zeta g\sin(\Phi/2)$, with $\zeta > 0.5$ a dimensionless parameter. In this regime, the critical spin state is simplified to $|\sigma_c\rangle = \frac{1}{\sqrt{2}}(|\downarrow\rangle - \mathrm{sgn}(\varepsilon)|\uparrow\rangle)$, featuring equal probabilities in both spin states. This characteristic polarization can serve as a clear experimental signature of the critical point. To quantify the system's sensitivity to the synthetic magnetic flux, we compute the quantum Fisher information (QFI) $\mathcal{F}$ as a function of Φ [see Fig. 2(c)]. According to the Cramér-Rao bound, the QFI sets the ultimate precision limit for estimating Φ, with its variance $\mathrm{Var}(\Phi) \geqslant \mathcal{F}^{-1}$ [53–55]. In particular, $\mathcal{F}$ diverges as the system approaches the quantum critical point, highlighting its potential metrological advantage.

As the system crosses the quantum critical point, both the spin and the cavity field exhibit bimodality, a signature of the underlying symmetry-breaking phase transition [14] [see Figs. 2(d)–2(f)]. This behavior is revealed by solving the semiclassical Maxwell-Bloch equations for a damped cavity,

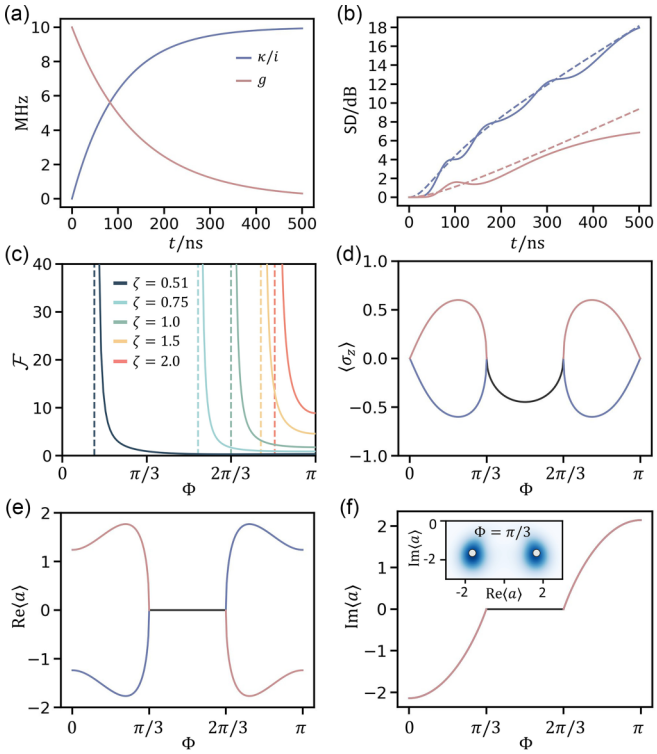


FIG. 2. Critical cavity field squeezing and spin polarization. (a) Variation of the system parameters during the squeezing protocol at $\Phi = \pi$. (b) Time evolution of the squeezing degree (SD). The blue (red) curves correspond to $\Phi = \pi$ ($\Phi = 0$). Solid lines show numerical results obtained by solving the time-dependent Schrödinger equation, while dashed lines denote the ideal squeezing degree of the instantaneous zeroth eigenstate. (c) The QFI as a function of Φ near the critical point, constrained by $\varepsilon = \zeta g \cos(\Phi/2)$ and $\kappa = i\zeta g \sin(\Phi/2)$. Panels (d), (e), and (f) are $\langle\sigma_z\rangle$, $\mathrm{Re}\langle a\rangle$, and $\mathrm{Im}\langle a\rangle$ in the steady state with $\zeta = 1$, i.e., on the solid line in Fig. 1(a). The red and blue lines correspond to the two steady-state solutions in the continuous-spectrum phase. The inset in panel (f) shows the Wigner distribution of the steady-state cavity field at $\Phi = \pi/3$. The white dots mark the values of $\langle a\rangle$ solved in the semiclassical approach. We set the cavity loss rate $\gamma = 0.35g$ and $\Delta = 0$ in the simulation.

which yield two distinct steady-state solutions (see the Supplemental Material [49]). In the continuous phase, we obtain dual-valued spin polarization $\langle\sigma_z\rangle$, accompanied by cavity fields with identical amplitudes but distinct phases. These reflect the underlying bistability of the coupled light-matter system. The inset in Fig. 2(f) shows the Wigner distribution of the steady state obtained by numerically solving the Lindblad master equation. The numerical results closely match the semiclassical steady-state solutions, indicated by the two white dots.

V. TOPOLOGICAL EDGE STATES

When $\varepsilon = 0$, the Hamiltonian in Eq. (1) can be represented by a Bloch sphere. In this case, the zeroth eigenstate has a topological origin, emerging at the boundary between two distinct topological phases, characterized by the projected winding numbers in the absence of chiral (sublattice) symmetry [45]. To illustrate this, we take $\varepsilon = 0$ in Eq. (5) to obtain $H_n(k) = \mathbf{d}_n(k) \cdot \boldsymbol{\sigma}$ with $\mathbf{d}_n(k) = (\mathrm{Re}[g\sqrt{n}e^{ik} + \eta],$ $-\mathrm{Im}[g\sqrt{n}e^{ik} + \eta],$ $2\mathrm{Re}[\kappa^*\sqrt{n}e^{ik}])$. The presence of the σ_z component breaks chiral symmetry. Thus, the topological phases cannot be represented by the winding number in the Su-Schrieffer-Heeger model [38,56,57]. Instead, the topological classification based on the projected winding numbers [45] can be understood geometrically by analyzing whether the closed trajectory of $\mathbf{d}_n(k)$ as k varies from 0 to 2π encloses the projected origin in its plane, as illustrated in Fig. 3(a). The system's topological phase depends on the photon number n. In the FSL, there exist two topologically distinct phases, separated by a critical photon number n_c. To determine n_c, we calculate the projected origin in the trajectory plane, given by $\mathbf{O}' = u\,(-2\mathrm{Re}[\kappa],\ 2\mathrm{Im}[\kappa],\ g)$, where $u = -(\kappa\eta^* + \kappa^*\eta)/(g^2 + 4|\kappa|^2)$. At the topological transition point, the trajectory $\mathbf{d}_{n_c}(k)$ passes through $\mathbf{O}'$, leading to the condition $g\sqrt{n_c}e^{ik} + \eta = -2\kappa u$. We obtain

$$n_c = \left| \frac{2\kappa(\kappa\eta^* + \kappa^*\eta)}{g(g^2 + 4|\kappa|^2)} - \frac{\eta}{g} \right|^2, \tag{9}$$

which is consistent with Eq. (7a) for $\varepsilon = 0$, i.e., $n_c = |\alpha_0 + \alpha_s|^2$. Therefore, the zeroth eigenstate is a topological edge state. In Fig. 3(b), we present the energy spectrum as a

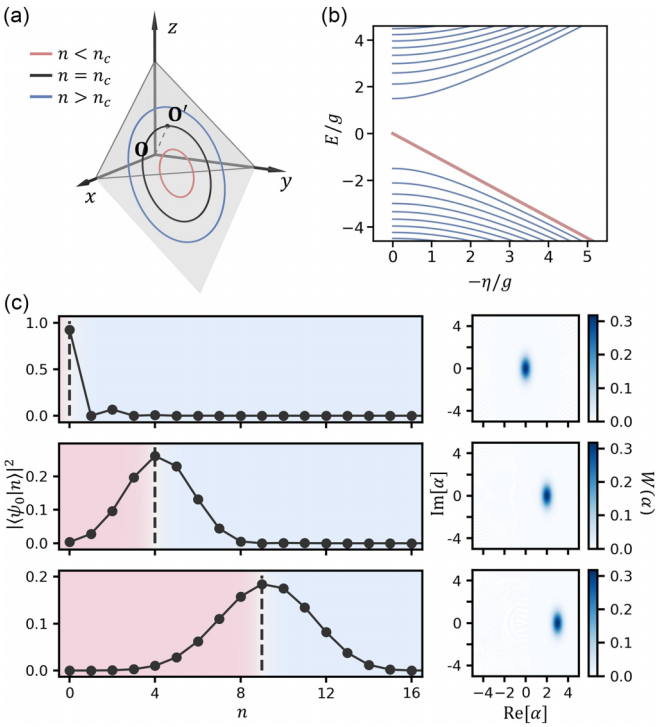


FIG. 3. The topological edge states. (a) Generalized topological classification with broken chiral symmetry. For different n, the trajectories of $\mathbf{d}_n(k)$ form a plane (shaded area). The origin $\mathbf{O}$ has a projected point $\mathbf{O}'$ in this plane. For the topological critical photon number n_c, the projected origin $\mathbf{O}'$ locates on the trajectory of $\mathbf{d}_{n_c}(k)$ (black curve). (b) The energy spectra as a function of η. The zeroth eigenenergy is highlighted in red color. (c) Fock-space (left panel) and phase-space (right panel) distribution of the generalized topological edge state. The red and blue colors highlight the topologically trivial and nontrivial phases, respectively. From top to bottom, $\eta/g = 0, -10$, and -15. In the left panel, the black dashed lines mark the topological edge. We set $\kappa = g$.

function of η, demonstrating the breaking of chiral symmetry induced by a finite κ. This symmetry breaking is evidenced by the asymmetric position of the zeroth energy level in the spectra. In Fig. 3(c), we show the Fock-state occupation of the zeroth eigenstate, obtained by tracing out the sublattice degree of freedom. The result reveals that the state is exponentially localized around the topological critical point (marked by the black dashed line). In an experiment, this edge state can be detected through photon-number distribution tomography.

In summary, we have investigated QPTs in driven JC FSLs under a synthetic gauge field, uncovering its critical behavior, topological characteristics, and potential applications in generating squeezed fields. While driving fields have been employed in the Dicke [58,59] and Tavis-Cummings [5] models to achieve effective ultrastrong couplings and induce QPTs, in our case, the driving field plays a qualitatively different role by introducing a synthetic gauge field that significantly enriches the phase diagram. Our model can be viewed as an extension of the minimal Harper-Hofstadter model [39] with the addition of the JC coupling term, which acts like a disorder that leads to the localized oscillating states and the insulating (discrete-spectrum) phase. Looking forward, this framework can be extended in multiple directions, such as incorporating off-resonant driving fields [14] or introducing additional cavity modes [37] to explore higher-dimensional and more complex quantum phases.

ACKNOWLEDGMENTS

This work was supported by the National Key Research and Development Program of China (Grant No. 2024YFA1408900), the National Natural Science Funds for Distinguished Young Scholar (Grant No. 12325412), the National Natural Science Foundation of China (Grant No. 12434020), the China National Postdoctoral Program for Innovative Talents (Grant No. BX20240302), the Fundamental Research Funds for the Central Universities (Grant No. 2024FZZX02-01-02), and the Quantum Science and Technology-National Science and Technology Major Project (Grant No. 2021ZD0303200).

DATA AVAILABILITY

The data that support the findings of this article are openly available [60].

[1] M. Uhlarz, C. Pfleiderer, and S. M. Hayden, Quantum phase transitions in the itinerant ferromagnet $ZrZn_2$, Phys. Rev. Lett. **93**, 256404 (2004).

[2] S. Sachdev, *Colloquium*: Order and quantum phase transitions in the cuprate superconductors, Rev. Mod. Phys. **75**, 913 (2003).

[3] Y. K. Wang and F. T. Hioe, Phase transition in the Dicke model of superradiance, Phys. Rev. A **7**, 831 (1973).

[4] V. M. Bastidas, C. Emary, B. Regler, and T. Brandes, Nonequilibrium quantum phase transitions in the Dicke model, Phys. Rev. Lett. **108**, 043003 (2012).

[5] M. Feng, Y. Zhong, T. Liu, L. Yan, W. Yang, J. Twamley, and H. Wang, Exploring the quantum critical behavior in a driven Tavis–Cummings circuit, Nat. Commun. **6**, 7111 (2015).

[6] C. J. Zhu, L. L. Ping, Y. P. Yang, and G. S. Agarwal, Squeezed light induced symmetry breaking superradiant phase transition, Phys. Rev. Lett. **124**, 073602 (2020).

[7] M.-J. Hwang and M. B. Plenio, Quantum phase transition in the finite Jaynes-Cummings lattice systems, Phys. Rev. Lett. **117**, 123602 (2016).

[8] M.-J. Hwang, R. Puebla, and M. B. Plenio, Quantum phase transition and universal dynamics in the Rabi model, Phys. Rev. Lett. **115**, 180404 (2015).

[9] M. Liu, S. Chesi, Z.-J. Ying, X. Chen, H.-G. Luo, and H.-Q. Lin, Universal scaling and critical exponents of the anisotropic quantum Rabi model, Phys. Rev. Lett. **119**, 220601 (2017).

[10] M.-L. Cai, Z.-D. Liu, W.-D. Zhao, Y.-K. Wu, Q.-X. Mei, Y. Jiang, L. He, X. Zhang, Z.-C. Zhou, and L.-M. Duan, Observation of a quantum phase transition in the quantum Rabi model with a single trapped ion, Nat. Commun. **12**, 1126 (2021).

[11] R.-H. Zheng, W. Ning, Y.-H. Chen, J.-H. Lü, L.-T. Shen, K. Xu, Y.-R. Zhang, D. Xu, H. Li, Y. Xia, F. Wu, Z.-B. Yang, A. Miranowicz, N. Lambert, D. Zheng, H. Fan, F. Nori, and S.-B. Zheng, Observation of a superradiant phase transition with emergent cat states, Phys. Rev. Lett. **131**, 113601 (2023).

[12] P. Alsing and H. Carmichael, Spontaneous dressed-state polarization of a coupled atom and cavity mode, Quantum Opt.: J. Eur. Opt. Soc. Part B **3**, 13 (1991).

[13] P. Alsing, D.-S. Guo, and H. J. Carmichael, Dynamic Stark effect for the Jaynes-Cummings system, Phys. Rev. A **45**, 5135 (1992).

[14] H. J. Carmichael, Breakdown of photon blockade: A dissipative quantum phase transition in zero dimensions, Phys. Rev. X **5**, 031028 (2015).

[15] J. M. Fink, A. Dombi, A. Vukics, A. Wallraff, and P. Domokos, Observation of the photon-blockade breakdown phase transition, Phys. Rev. X **7**, 011012 (2017).

[16] R. Sett, F. Hassani, D. Phan, S. Barzanjeh, A. Vukics, and J. M. Fink, Emergent macroscopic bistability induced by a single superconducting qubit, PRX Quantum **5**, 010327 (2024).

[17] J.-H. Lü, W. Ning, F. Wu, R.-H. Zheng, K. Chen, X. Zhu, Z.-B. Yang, H.-Z. Wu, and S.-B. Zheng, Critical quantum metrology robust against dissipation and non-adiabaticity, arXiv:2403.04475.

[18] P. Grangier, R. E. Slusher, B. Yurke, and A. LaPorta, Squeezed-light-enhanced polarization interferometer, Phys. Rev. Lett. **59**, 2153 (1987).

[19] M. Xiao, L.-A. Wu, and H. J. Kimble, Precision measurement beyond the shot-noise limit, Phys. Rev. Lett. **59**, 278 (1987).

[20] LIGO Scientific Collaboration, A gravitational wave observatory operating beyond the quantum shot-noise limit, Nat. Phys. **7**, 962 (2011).

[21] F. Li, T. Li, M. O. Scully, and G. S. Agarwal, Quantum advantage with seeded squeezed light for absorption measurement, Phys. Rev. Appl. **15**, 044030 (2021).

[22] T. Li, F. Li, X. Liu, V. V. Yakovlev, and G. S. Agarwal, Quantum-enhanced stimulated Brillouin scattering spectroscopy and imaging, Optica **9**, 959 (2022).

[23] J. Qin, Y.-H. Deng, H.-S. Zhong, L.-C. Peng, H. Su, Y.-H. Luo, J.-M. Xu, D. Wu, S.-Q. Gong, H.-L. Liu, H. Wang, M.-C. Chen,

L. Li, N.-L. Liu, C.-Y. Lu, and J.-W. Pan, Unconditional and robust quantum metrological advantage beyond N00N states, Phys. Rev. Lett. **130**, 070801 (2023).

[24] T. Gehring, V. Händchen, J. Duhme, F. Furrer, T. Franz, C. Pacher, R. F. Werner, and R. Schnabel, Implementation of continuous-variable quantum key distribution with composable and one-sided-device-independent security against coherent attacks, Nat. Commun. **6**, 8795 (2015).

[25] I. Derkach, V. C. Usenko, and R. Filip, Squeezing-enhanced quantum key distribution over atmospheric channels, New J. Phys. **22**, 053006 (2020).

[26] O. Thearle, J. Janousek, S. Armstrong, S. Hosseini, M. Schünemann (Mraz), S. Assad, T. Symul, M. R. James, E. Huntington, T. C. Ralph, and P. K. Lam, Violation of Bell's inequality using continuous variable measurements, Phys. Rev. Lett. **120**, 040406 (2018).

[27] Y. Wu, J. Yuan, C. Zhang, Z. Zhu, J. Deng, X. Zhang, P. Zhang, Q. Guo, Z. Wang, J. Huang, C. Song, H. Li, D.-W. Wang, H. Wang, and G. S. Agarwal, Testing the unified bounds of the quantum speed limit, Phys. Rev. A **110**, 042215 (2024).

[28] D. Sharma and B. Kumar, Power-law growth of time and strength of squeezing near a quantum critical point, Phys. Rev. A **102**, 033702 (2020).

[29] K. Gietka, Squeezing by critical speeding up: Applications in quantum metrology, Phys. Rev. A **105**, 042620 (2022).

[30] K. Hayashida, T. Makihara, N. Marquez Peraca, D. Fallas Padilla, H. Pu, J. Kono, and M. Bamba, Perfect intrinsic squeezing at the superradiant phase transition critical point, Sci. Rep. **13**, 2526 (2023).

[31] T. Roscilde, F. Caleca, A. Angelone, and F. Mezzacapo, Scalable spin squeezing from critical slowing down in short-range interacting systems, Phys. Rev. Lett. **133**, 210401 (2024).

[32] D.-W. Wang, H. Cai, R.-B. Liu, and M. O. Scully, Mesoscopic superposition states generated by synthetic spin-orbit interaction in Fock-state lattices, Phys. Rev. Lett. **116**, 220502 (2016).

[33] H. Cai and D. W. Wang, Topological phases of quantized light, Nat. Sci. Rev. **8**, nwaa196 (2021).

[34] P. Saugmann and J. Larson, Fock-state-lattice approach to quantum optics, Phys. Rev. A **108**, 033721 (2023).

[35] J. Yuan, H. Cai, and D.-W. Wang, Quantum simulation in Fock-state lattices, Adv. Phys. X **9**, 2325611 (2024).

[36] J. Yang, Y. Li, Y. Yang, X. Xie, Z. Zhang, J. Yuan, H. Cai, D.-W. Wang, and F. Gao, Realization of all-band-flat photonic lattices, Nat. Commun. **15**, 1484 (2024).

[37] M. Peng, Q. Wei, J. Yuan, D.-W. Wang, M. Yan, H. Cai, and G. Chen, Ideal flat and resolved SU(3) Landau levels in three dimensions, Phys. Rev. Lett. **134**, 116601 (2025).

[38] J. Deng, H. Dong, C. Zhang, Y. Wu, J. Yuan, X. Zhu, F. Jin, H. Li, Z. Wang, H. Cai, C. Song, H. Wang, J. Q. You, and D.-W. Wang, Observing the quantum topology of light, Science **378**, 966 (2022).

[39] Y. Wang, Y.-K. Wu, Y. Jiang, M.-L. Cai, B.-W. Li, Q.-X. Mei, B.-X. Qi, Z.-C. Zhou, and L.-M. Duan, Realizing synthetic dimensions and artificial magnetic flux in a trapped-ion quantum simulator, Phys. Rev. Lett. **132**, 130601 (2024).

[40] J. Zhang, W. Huang, J. Chu, J. Qiu, X. Sun, Z. Tao, J. Zhang, L. Zhang, Y. Zhou, Y. Chen, Y. Liu, S. Liu, Y. Zhong, J.-J. Miao, J. Niu, and D. Yu, Synthetic multidimensional Aharonov-Bohm cages in Fock state lattices, Phys. Rev. Lett. **134**, 070601 (2025).

[41] J. Yuan, C. Xu, H. Cai, and D. W. Wang, Gap-protected transfer of topological defect states in photonic lattices, APL Photonics **6**, 030803 (2021).

[42] J. Yuan, H. Cai, C. Wu, S.-Y. Zhu, R.-B. Liu, and D.-W. Wang, Unification of valley and anomalous Hall effects in a strained lattice, Phys. Rev. B **104**, 035410 (2021).

[43] C. Wu, W. Liu, Y. Jia, G. Chen, and F. Chen, Observation of topological pumping of a defect state in a Fock photonic lattice, Phys. Rev. A **107**, 033501 (2023).

[44] T. Tian, H. Cai, L. Zhang, Y. Zhang, C.-K. Duan, and J. Zhou, Nonadiabatic topological transfer in a nanomechanical phononic lattice, Phys. Rev. B **109**, 125123 (2024).

[45] Q. Wang and N. Hao, Generalized topology in lattice models without chiral symmetry, arXiv:2407.00795.

[46] D.-W. Wang, C. Song, W. Feng, H. Cai, D. Xu, H. Deng, H. Li, D. Zheng, X. Zhu, H. Wang *et al.*, Synthesis of antisymmetric spin exchange interaction and chiral spin clusters in superconducting circuits, Nat. Phys. **15**, 382 (2019).

[47] W. Liu, W. Feng, W. Ren, D.-W. Wang, and H. Wang, Synthesizing three-body interaction of spin chirality with superconducting qubits, Appl. Phys. Lett. **116**, 114001 (2020).

[48] N. Goldman and J. Dalibard, Periodically driven quantum systems: Effective Hamiltonians and engineered gauge fields, Phys. Rev. X **4**, 031027 (2014).

[49] See Supplemental Material at http://link.aps.org/supplemental/10.1103/4fq1-nb4r for model diagonalization, Floquet effective Hamiltonian, quasi-momentum-space description, and steady-state solution.

[50] V. M. Pereira, A. H. Castro Neto, and N. M. R. Peres, Tight-binding approach to uniaxial strain in graphene, Phys. Rev. B **80**, 045401 (2009).

[51] Y.-H. Ho, E. V. Castro, and M. A. Cazalilla, Haldane model under nonuniform strain, Phys. Rev. B **96**, 155446 (2017).

[52] C.-K. Chiu, J. C. Y. Teo, A. P. Schnyder, and S. Ryu, Classification of topological quantum matter with symmetries, Rev. Mod. Phys. **88**, 035005 (2016).

[53] Y. Tang, Y. Yang, M. An, J. Xie, Y. Wang, F. Wang, and F. Li, Critical properties of quantum Fisher information of SU(1,1)-dynamic systems, Phys. Rev. A **110**, 022611 (2024).

[54] Y. Yang, H. Yuan, and F. Li, Quantum multiparameter estimation enhanced by a topological phase transition, Phys. Rev. A **109**, 022604 (2024).

[55] C. Hotter, H. Ritsch, and K. Gietka, Combining critical and quantum metrology, Phys. Rev. Lett. **132**, 060801 (2024).

[56] W. P. Su, J. R. Schrieffer, and A. J. Heeger, Solitons in polyacetylene, Phys. Rev. Lett. **42**, 1698 (1979).

[57] E. J. Meier, F. A. An, and B. Gadway, Observation of the topological soliton state in the Su–Schrieffer–Heeger model, Nat. Commun. **7**, 13986 (2016).

[58] K. Baumann, C. Guerlin, F. Brennecke, and T. Esslinger, Dicke quantum phase transition with a superfluid gas in an optical cavity, Nature (London) **464**, 1301 (2010).

[59] M. P. Baden, K. J. Arnold, A. L. Grimsmo, S. Parkins, and M. D. Barrett, Realization of the Dicke model using cavity-assisted Raman transitions, Phys. Rev. Lett. **113**, 020408 (2014).

[60] J. Yuan, J. Deng, X. Wei, and D.-W. Wang, Quantum phase transitions in driven Fock-state lattices with synthetic gauge fields [Data set], Zenodo (2025), doi: 10.5281/zenodo.16279175.